ELECTRIC AND MAGNETIC FIELD MEASUREMENTS OF MHD MODES IN THE BERKELEY MULTIPLE MIRROR

by

R. Close

Memorandum No. UCB/ERL M85/49

12 June 1985

ELECTRONICS RESEARCH LABORATORY

College of Engineering
University of California, Berkeley
94720

ELECTRIC AND MAGNETIC FIELD MEASUREMENTS OF MHD MODES IN THE BERKELEY MULTIPLE MIRROR

Robert Close

May 18, 1985

ABSTRACT

Diagnostic systems have been developed for the measurement of the electric and magnetic fields which arise from instabilities in the Berkeley Multiple Mirror Experiment (MMX). Floating potential measurements from an array of high-impedance probes are used to calculate electric field fluctuations and $\vec{E} \times \vec{B}$ drifts associated with curvature-driven instabilities. A pair of compensated magnetic probes is used to measure magnetic fluctuations associated with ballooning modes.

1 INTRODUCTION

The Berkeley Multiple Mirror is being used to study stability limits of curvature-driven high-β ballooning modes [[1]-[4]]. Finite ion Larmor radius (FLR) effects appear to stabilize azimuthal modes $m > 1$, so that only the $m = 1$ displacement mode is observed. FLR effects force the $m = 1$ mode to have a nearly rigid radial profile [[5]]. The diagnostics described in this report are specifically designed for study of this mode, although the techniques can be generalized to the study of higher azimuthal mode numbers.

For the experiments reported here, an axisymmetric multiple mirror is average-minimum-B stabilized by cusp fields at the ends of a variable number of simple mirror cells. Theta pinch and Marshall gun sources inject counter-streaming plasmas along a solenoid simultaneous with the application of the mirror and cusp fields (see Figure 1). The plasmas thermalize to yield $10^{14} \leq n \leq 10^{15}$ cm^{-3} and $5 \leq T \leq 20$ eV ($\beta \leq 15\%$). Balloning instabilities are studied in the resulting transient ($\tau \approx 40\mu$s) high-β plasma.

1.1 Plasma centroid motion from ion saturation current measurements

The polar position of the center of the plasma distribution is determined from measurements of ion saturation currents by an azimuthal array of Langmuir probes (Figure 2). For $T = T_e = T_i$ the Bohm sheath criterion is

satisfied, and in the absence of flow the ion current is related to the density by the equation:

$$I_+ = i_+ \frac{ZenAv_{Ti}}{4} \tag{1}$$

where $Z = 1$ for hydrogen, A is the probe surface area, $v_{Ti} = (8kT/\pi M)^{1/2}$ is the ion thermal speed, and $i_+(T, V, n)$ is the Laframboise correction to the random ion flux [[7]]. The temperature is assumed uniform across the plasma, and the density distribution is assumed to be gaussian:

$$n = n_0 \exp\left\{\frac{(x - x_0)^2}{r_x^2} + \frac{(y - y_0)^2}{r_y^2}\right\} \tag{2}$$

where (x, y) is the probe position, (x_0, y_0) is the plasma centroid position, and the plasma radius is given by $r_p^2 = r_x r_y$. Eccentricty oriented along the x, y axes can be calculated from r_x and r_y. Because deviations from the assumed gaussian profile can result in spurious eccentricities, r_x and r_y are set equal to the plasma radius r_p for calculation of the $m = 1$ centroid displacement. The plasma density profile is calculated from measurements made by Langmuir probes at four different radii and fitted to a Gaussian to determine r_p (Figure 3).. The motion of the plasma is determined by solving equations 2 for (x_0, y_0).

1.2 Observation of instabilities

By comparing the plasma centroid motion at different axial positions, we can distinguish between flutelike and ballooning instabilities. Examples of stable, flutelike, and ballooning behavior are shown in Figures 4- 6. Flute instabilities have nearly uniform displacement along the axis, while ballooning instabilities are characterized by an axial variation in the displacement mode amplitude.

2 ELECTRIC FIELD DETERMINATION

2.1 Model of electrostatic potential formation

We consider two causes of electric fields in the plasma: (1) a radial ambipolar field, and (2) a uniform field which results from charge drifts in the curved magnetic field. The total potential is a superposition of the potentials from each of these effects.

Diffusion in the multiple mirror gives rise to ambipolar potentials in two ways. First, ambipolar diffusion parallel to $\vec{B}$ produces a positive potential in the plasma due to the faster escape of electrons. Second, ion-ion radial diffusion produces a potential minimum on axis, with a radially inward electric field. Note that collisions between ions and electrons give rise to radial diffusion, but do not cause charge separation and therefore do not affect the radial potential profile.

It is shown in Appendix A that ion-ion diffusion in a uniform temperature plasma will produce a potential profile which scales with density like $\Phi \propto n^2/r_p^4$. For a plasma expanding radially, $r_p^4 \propto n^{-2}$, so $\Phi \propto n^4$ and the decay times τ_Φ and τ_n are related by $\tau_\Phi \approx \tau_n/4$. By contrast, radial electron temperature differences would not decay with any functional relationship to density.

In the sharp-boundary limit, the $m = 1$ instability has a dipole charge distribution. This results in a uniform electric field $\vec{E}^1$ across the plasma, so that the plasma moves almost rigidly. We assume that the diffuse-boundary ballooning mode will also be have a rigid radial profile because of FLR effects [[5]].

As the plasma (position $\vec{r}_0 = (x_0, y_0)$) moves inside the stainless steel chamber, image charges hold the potential fixed near the conducting wall. Therefore the shape of the radial potential profile changes as the plasma moves. This behavior is approximated by assuming that as the plasma moves off-center, the change in potential at a fixed point differs from the change due simply to translation of the profile by a factor $\left(1 - \frac{r^2}{w^2}\right)$, where w is the wall radius. If the initially centered profile is parabolic:

$$\Phi(r) = \Phi_0 + \sigma r^2 \tag{3}$$

then the change of potential at a fixed r due to plasma motion is:

$$\triangle\Phi(r) = \left(1 - \frac{r^2}{w^2}\right)\sigma\left(|\vec{r} - \vec{r_0}|^2 - r^2\right) \tag{4}$$

Summing the initially centered potential profile, the change due to translation, and the instability potential $-\vec{E}\cdot\vec{r}$ gives:

$$\Phi(r) = \Phi_0 + \sigma r^2 + \left(1 - \frac{r^2}{w^2}\right)\sigma\left(|\vec{r} - \vec{r_0}|^2 - r^2\right) - \vec{E}\cdot\vec{r} \tag{5}$$

Using eight probes arrayed as in Figure 7, and labelling the potentials at each point by Φ_1, Φ_2,..., the equations above can be solved to give the m=1 electric field:

$$\begin{aligned} E_x &= \left(\frac{w^2-r_1^2}{r_2^2-r_1^2}\right)\left(\frac{\Phi_7-\Phi_5}{2r_2}\right) - \left(\frac{w^2-r_2^2}{r_2^2-r_1^2}\right)\left(\frac{\Phi_3-\Phi_1}{2r_1}\right) \\ E_y &= \left(\frac{w^2-r_1^2}{r_2^2-r_1^2}\right)\left(\frac{\Phi_8-\Phi_6}{2r_2}\right) - \left(\frac{w^2-r_2^2}{r_2^2-r_1^2}\right)\left(\frac{\Phi_4-\Phi_2}{2r_1}\right) \end{aligned} \tag{6}$$

Note that if no wall were present we would expect:

$$\begin{aligned} E_x &= \frac{\Phi_7-\Phi_5}{2r_2} = \frac{\Phi_3-\Phi_1}{2r_1} \\ E_y &= \frac{\Phi_8-\Phi_6}{2r_2} = \frac{\Phi_4-\Phi_2}{2r_1} \end{aligned} \tag{7}$$

The electric fields are used to calculate $\vec{E}\times\vec{B}$ drifts which are compared with the plasma motion calculated from Langmuir probe ion saturation current measurements.

2.2 Floating potential measurement

The electric field in the plasma is calculated from floating potential measurements in an array of high-impedance floating probes (Figure 7). Figure 8 shows the time evolution of the ambipolar potential radial distribution

for a stable shot. A comparison of the potential difference between probes at $x = -1.0$ and $x = 0.0$ cm with density reveals a dependence $V \propto n^4$ early in time, when radial diffusion is the dominant loss mechanism (Figure 10). Later, as axial loss becomes more important, the dependence of floating potential on density is weakened. This behavior, which is observed consistently, confirms our model of a uniform-temperature plasma. The measurements used to determine the electric field are made at small radii ($r \leq 2.0$ cm) where the profile can be approximated by a parabola.

Figure 9 shows the radial potential profile along $\hat{x}$ for a flute-unstable plasma. In this case, the instability has produced an electric field in the $-\hat{x}$ direction, resulting in an $\vec{E} \times \vec{B}$ drift in the $-\hat{y}$ direction since $\vec{B}$ is in the $-\hat{z}$ direction in this experiment.

2.3 Experimental results

The floating potential measurements are used to calculate an $\vec{E} \times \vec{B}$ drift velocity which is compared to the velocity obtained from the Langmuir probe array measurements of Section 1.1. As shown in Figures 11-14, the two measurements of plasma motion are in good agreement until the plasma moves far off center, when neither method can be considered reliable because of the low plasma densities at the probes.

It is hoped that the electric field measurement will prove more versatile than the ion-saturation current measurements in diagnosing plasma instabilities. The electric field measurement should be less sensitive to the shape of the equilibrium density profile, and to localized pertubations not characteristic of the $m = 1$ displacement mode. Evidence of this is seen in Figure 11, where the velocity calcualted from the Langmuir probe array drops suddenly to zero as the plasma moves away from the axis, probably because of a sharper-than-gaussian profile. The $\vec{E} \times \vec{B}$ drift calculated from the floating probe array reveals a gradual decay of the instability electric field, which seems physically reasonable.

3 MAGNETIC FIELD MEASUREMENTS

Ballooning modes are characterized by axial variations of the mode amplitude. In ideal MHD, the magnetic field lines move and bend with the plasma, giving rise to a perturbed magnetic field $\vec{B}^1$ which is perpendicular to $\vec{B}_0$. For a background field $\vec{B}_0 = 2$ kGauss which is bent ~ 2 cm over a length 100 cm, the perturbed magnetic field will be $\vec{B}^1 \sim 40$ Gauss. Each component of this field can be measured and distinguished from the azimuthally symmetric background field using compensated magnetic probes placed 180° apart.

3.1 Measurement of perturbed magnetic fields

The voltage induced in a magnetic probe with N loops of area A by a time-varying $\vec{B}$ field is:

$$V = -NA\frac{\partial B_\perp}{\partial t} \tag{8}$$

Each magnetic probe consists of 80 turns of wire at an average diameter of .106 cm with a length of .5 cm (Figure 15). The calculated inductance is $L = 1.4\mu$H, and is in agreement with measurements made on a Tektronix Type 130 L-C meter. The effective area NA is calculated to be approximately 0.70 turns$\cdot$ cm^2. The probes were calibrated by measuring the voltage induced when placed in a solenoid with an oscillating magnetic field:

$$NA = \left|\frac{V}{\omega B}\right| \tag{9}$$

The resulting calibration for the two probes used are:

$$\begin{aligned}(NA)_1 &= .59 \text{ turns} \cdot \text{cm}^2 \\ (NA)_2 &= .57 \text{ turns} \cdot \text{cm}^2\end{aligned} \tag{10}$$

To compensate for the different probe calibrations, a voltage divider is used to decrease the signal from probe #1:

$$\frac{R_2}{R_1 + R_2} = \frac{.57}{.59} \tag{11}$$

For $R_2 = 78\Omega$, this gives $R_1 = 2.7\Omega$, which is the value used in taking data.

3.2 Experimental results

The measurements of the perturbed magnetic field are compared to the plasma motion calculated from Langmuir probe measurements in order to determine whether magnetic field line bending is produced by the mode as predicted by ideal MHD theory. Figure 16 shows a comparison of perturbed magnetic field and plasma motion for a flute-unstable plasma, which should not have any associated magnetic perturbation. Figure 17 compares the perturbed magnetic field and the plasma motion for a plasma stabilized against flutes (ballooning). A good correlation between the magnetic perturbation and the plasma motion is observed, indicating MHD ballooning. However, the magnetic field perturbation decays after $t \sim 50\mu$Sec, indicating finite resistivity.

4 CONCLUSIONS

The diagnostics described in this report have been used successfully to measure $\vec{E}$ and $\vec{B}$ fields associated with curvature-driven MHD instabilities. The $\vec{E} \times \vec{B}$ velocity of the plasma is in reasonable agreement with the velocity calculated from derivitives of the plasma position as determined from Langmuir probe measurements. The measured transverse magnetic fields correlate well with the presence of ballooning modes, as expected from MHD theory.

APPENDIX

A Floating potential due to diffusion

In order to justify our assumption of uniform temperature in the plasma, we must show that the variations in floating potential in the plasma are due to the existence of real space potential variations. The observed floating potential profiles, in particular the scaling with density, can be explained by the following model based on ambipolar diffusion. We assume a quasi-static situation $\left(\frac{d}{dt} \approx 0\right)$. Collisions between electrons and ions are naturally ambipolar and do not give rise to radial electric fields. Radial ion-ion diffusion does generate electric fields, and must be balanced by electron end loss to preserve quasineutrality. Only these fluxes are considered in determining the electric field. The electron momentum balance equation along $\hat{z}$ is:

$$0 = -\frac{dp_e}{dz} - enE_z - m_e n \nu_{ei} v_z^e \tag{12}$$

which yields the electron end flux:

$$\Gamma_z^e = -\frac{en}{m_e \nu_{ei}} E_z - \frac{T}{m_e \nu_{ei}} \frac{dn}{dz} \tag{13}$$

The ion flux due to ion-ion diffusion in an azimuthally symmetric cylidrical plasma is given by [[6]]:

$$\Gamma_r^i = \frac{3}{8} n r_{\mathrm{L}}^4 \nu_{ii} \frac{1}{r^2} \frac{\partial}{\partial r} \left[r^3 n^2 \frac{\partial}{\partial r} \left(\frac{1}{rn} \frac{\partial n}{\partial r} \right) \right] \tag{14}$$

Using quasineutrality $\nabla \cdot \vec{\Gamma}^e = \nabla \cdot \vec{\Gamma}^i$ gives:

$$\frac{d}{dz}\left\{-\frac{en_0}{m_e\nu_{ei}^{(0)}}E_z - \frac{n_0T}{m_e\nu_{ei}^{(0)}}\frac{1}{n}\frac{dn}{dz}\right\} = \frac{3r_L^4\nu_{ii}^{(0)}}{8n_0}\frac{1}{r}\frac{\partial}{\partial r}\left\{\frac{1}{r}\frac{\partial}{\partial r}\left[r^3n^2\frac{\partial}{\partial r}\left(\frac{1}{rn}\frac{\partial n}{\partial r}\right)\right]\right\} \tag{15}$$

For a given density profile, the potential can be determined by calculating E_z and integrating along z. A precise calculation of the potential profile requires sensitive knowledge of the density profile (accurate for four derivatives). However, by letting $\frac{\partial}{\partial r} \propto 1/r_p$, and $\frac{\partial}{\partial z} \propto 1/L$ (and using $\nu_{ii} \propto \nu_{ei} \propto n$), the scaling of the radial dependence of E_z is $E_z \propto n^2/r_p^4$. Since Φ is simply an integral along z of E_z, we also have $\Phi \propto n^2/r_p^4$. If radial diffusion (resulting from e-i collisions) is the dominant loss process, then $n \propto r_p^{-2}$ and $\Phi \propto n^4$.

References

[1] H.D. Price,N.M.P. Benjamin, B.K. Kang, A.J. Lichtenberg, and M.A. Lieberman, **Phys. Fluids 28**(1), 392-402 (1985).

[2] H.D. Price, *Confinement and Stability of a Plasma in Multiple Magnetic Mirrors*, Ph.D thesis, College of Engineering, University of California, Berkeley, November 1982.

[3] R. Close,B.K. Kang, and A.J. Lichtenberg, 'Ballooning Displacement Modes in an Axisymmetric Multiple Mirror',BULLETIN OF THE AMERICAN PHYSICAL SOCIETY **28**(8), 1048 (October 1983).

[4] R. Close, C.W. Hartman, H. Meuth, and A.J. Lichtenberg,'Ballooning Modes in an Axisymmetric Multiple Mirror',BULLETIN OF THE AMERICAN PHYSICAL SOCIETY **29(8)**, 1302 (October 1984).

[5] T.B. Kaiser and L.D. Pearlstein, **Phys. Fluids 28**(3) , 1003-1005 (1985).

[6] M.Tuszewski and A.J. Lichtenberg, **Phys. Fluids 20**(8), 1274 (1977).

[7] J.G. Laframboise, *Theory of Spherical and Cylindrical Langmuir Probes in a Collisionless, Maxwellian Plasma at Rest*, University of Toronto Institute for Aerospace Studies Report No. 100 (June 1966).

Acknowledgements

This work was supported by DOE Contract No. DE-ATO3-76ET53059. Thanks to A.J. Lichtenberg and B. Archer for their help in writing this report.

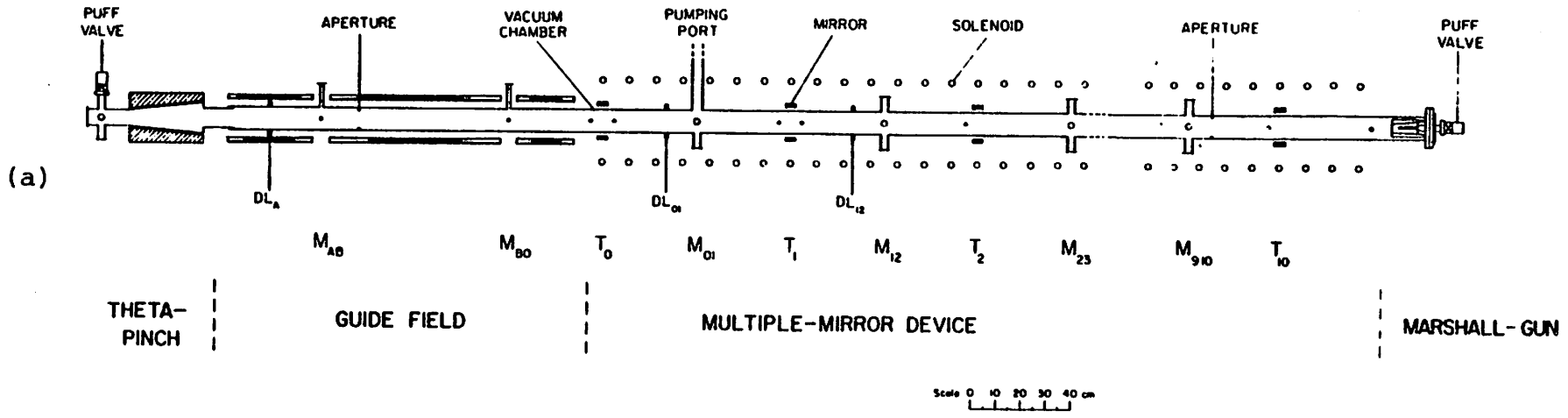

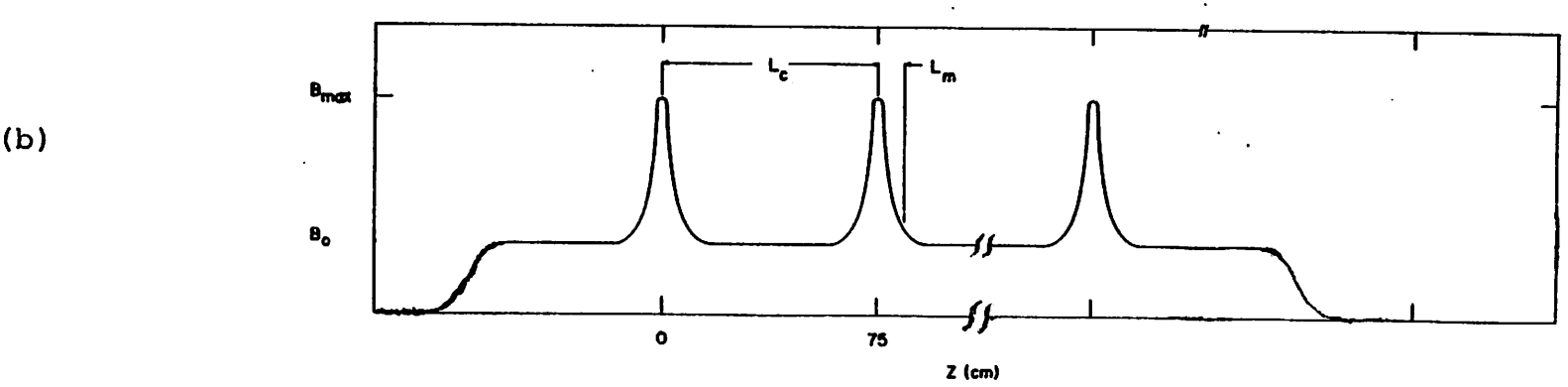

Figure 1: (a) Schematic of the 10 meter multiple-mirror device.
(b) Axial magnetic field profile.

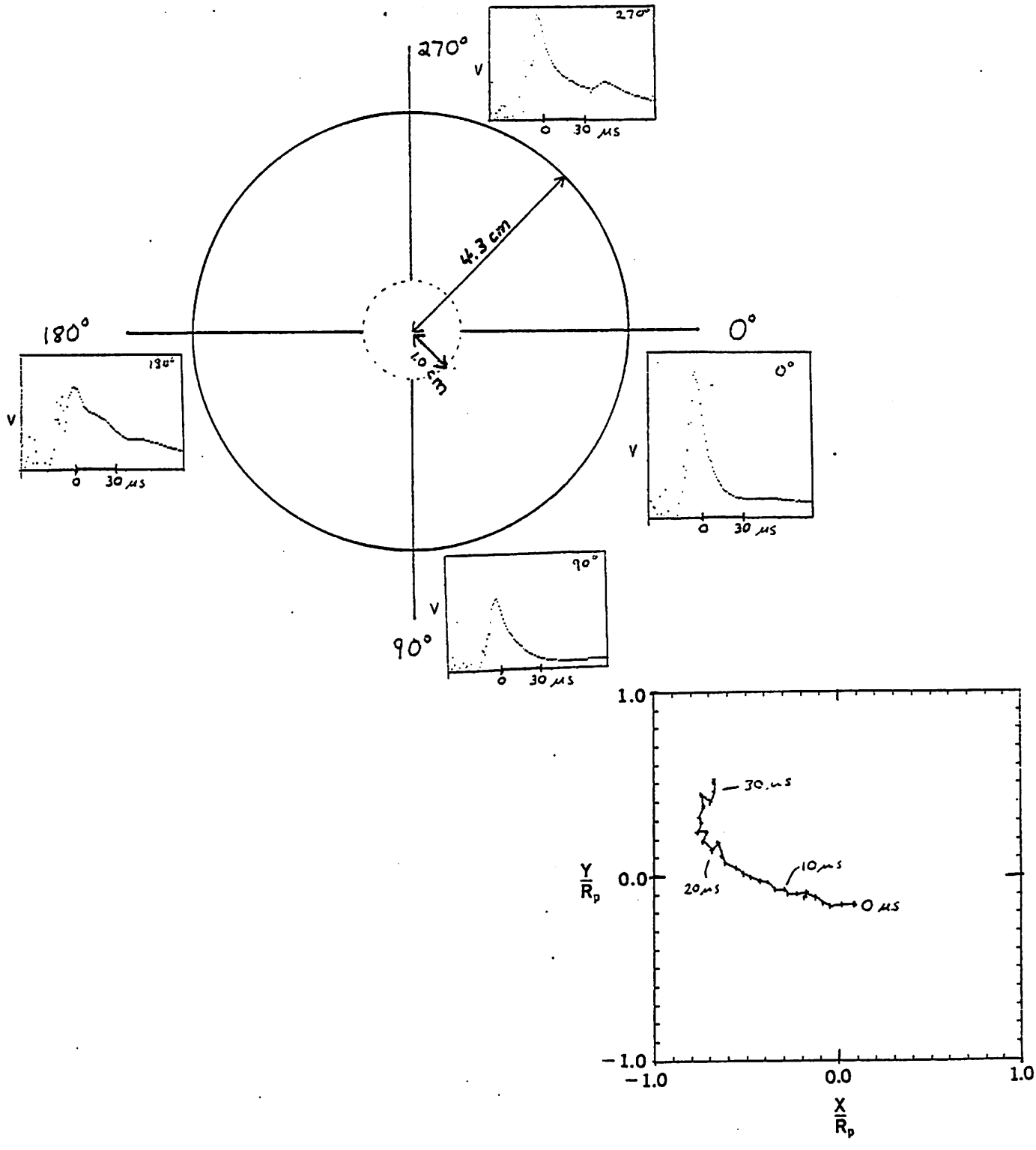

Figure 2: An array of Langmuir probes is used to calculate the pasma centroid motion. Cylindrical probe tips have $r = .0635$mm and $l = 1.02$mm.

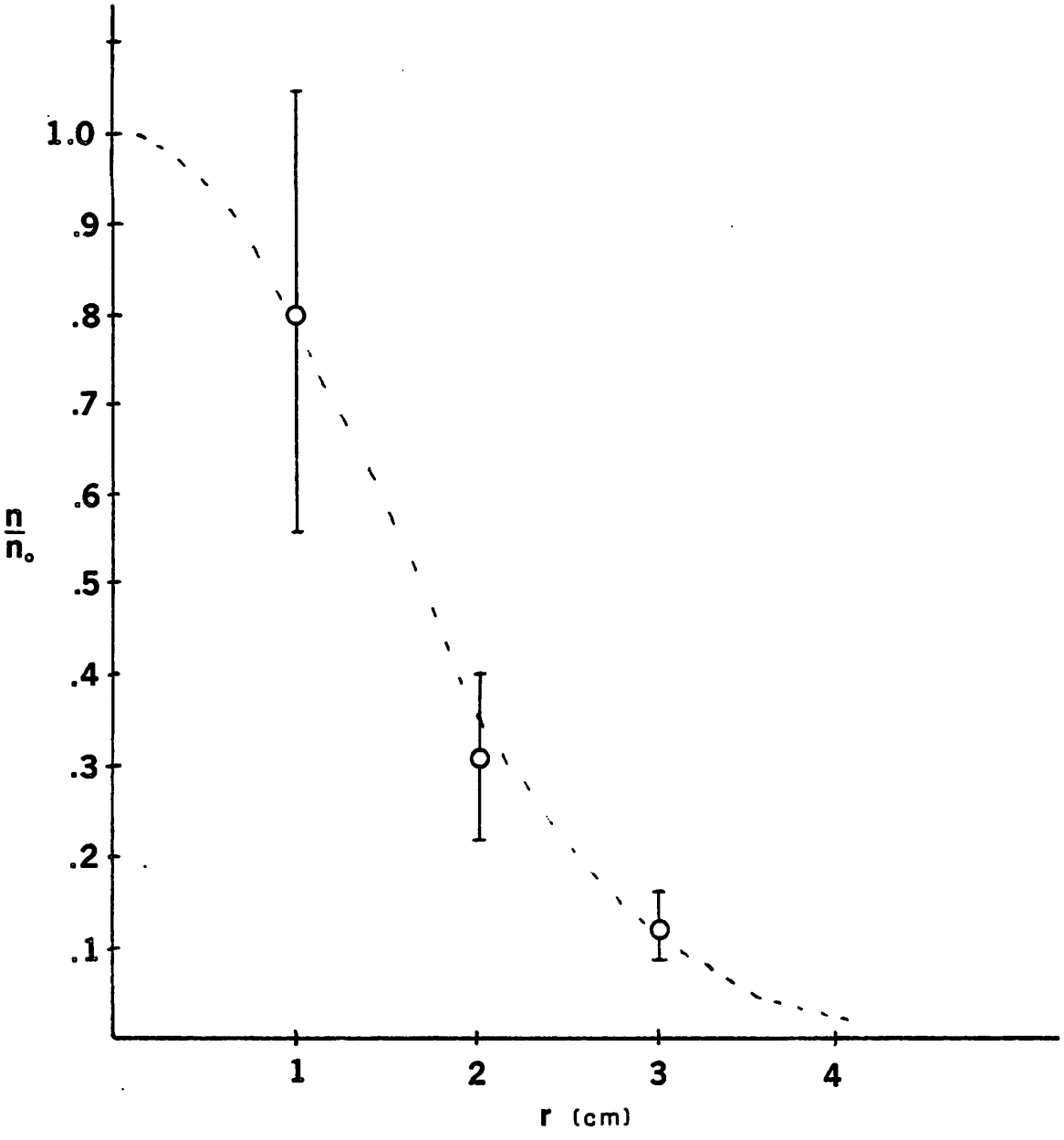

Figure 3: Normalized radial density profile.

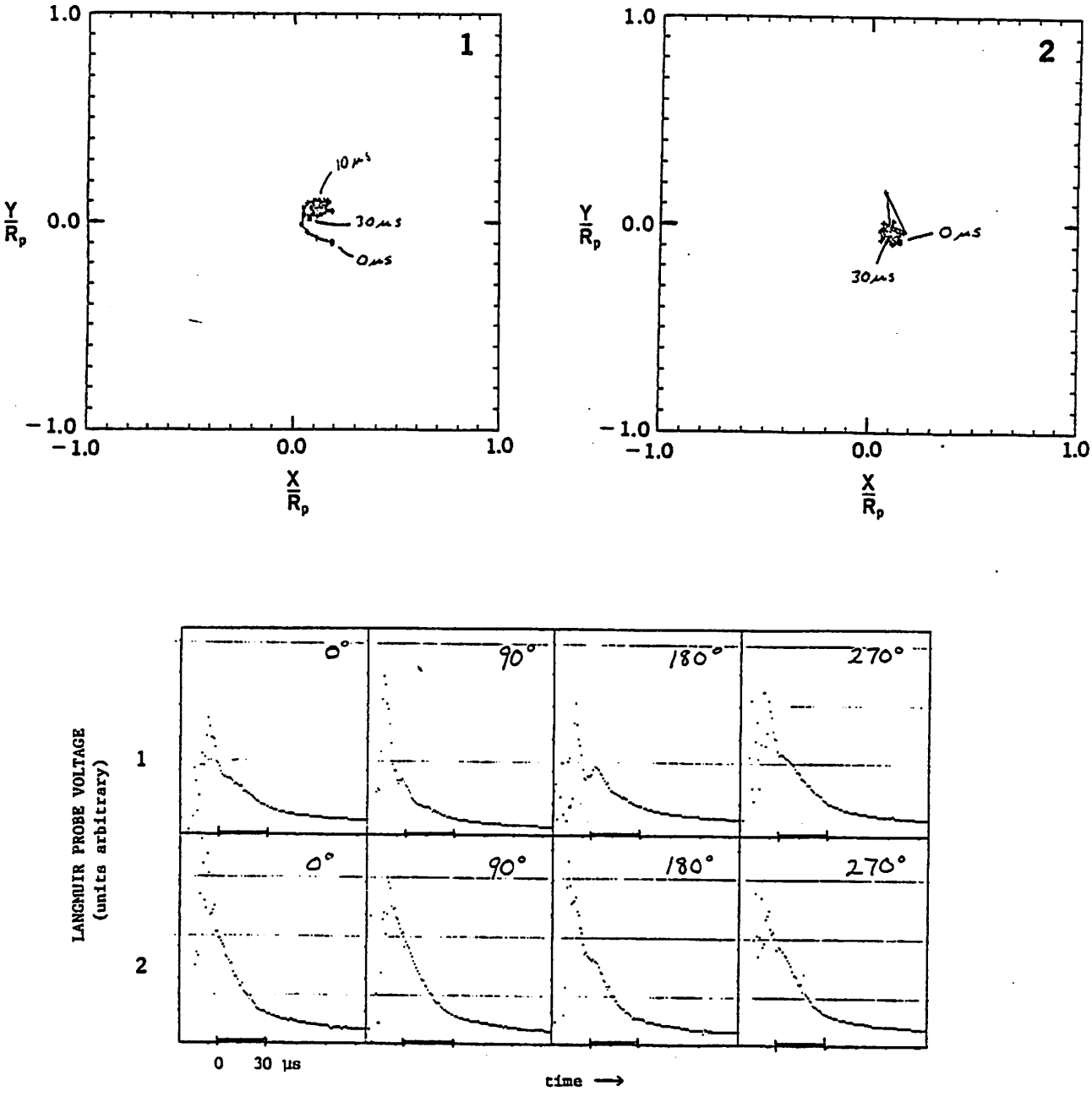

Figure 4: Centroid motion in a mirror cell (1) and near a cusp (2) calculated from Langmuir probe data for a stable plasma.

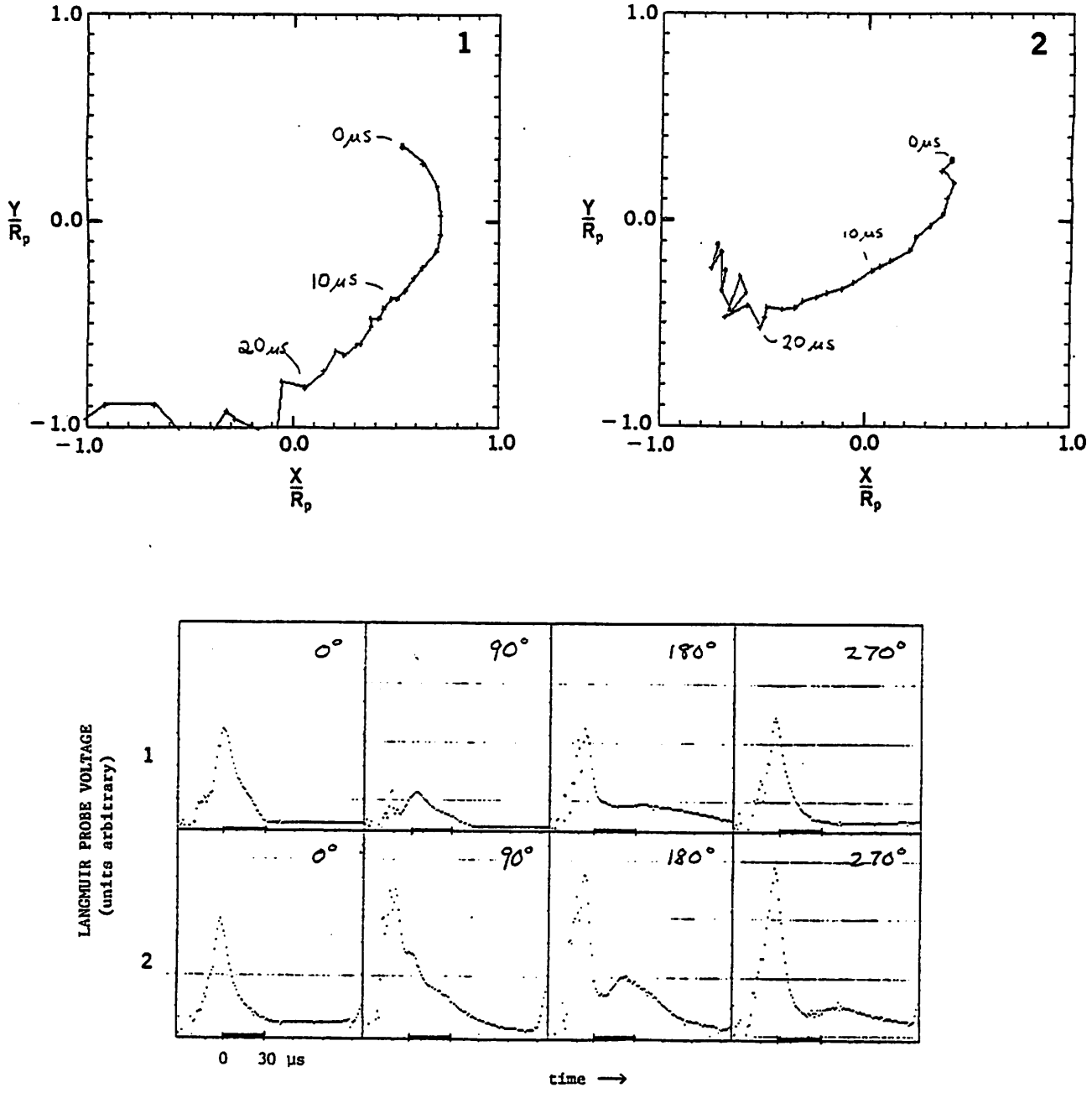

Figure 5: Centroid motion in a mirror cell (1) and a solenoid region (2) calculated from Langmuir probe data for a flute-unstable plasma.

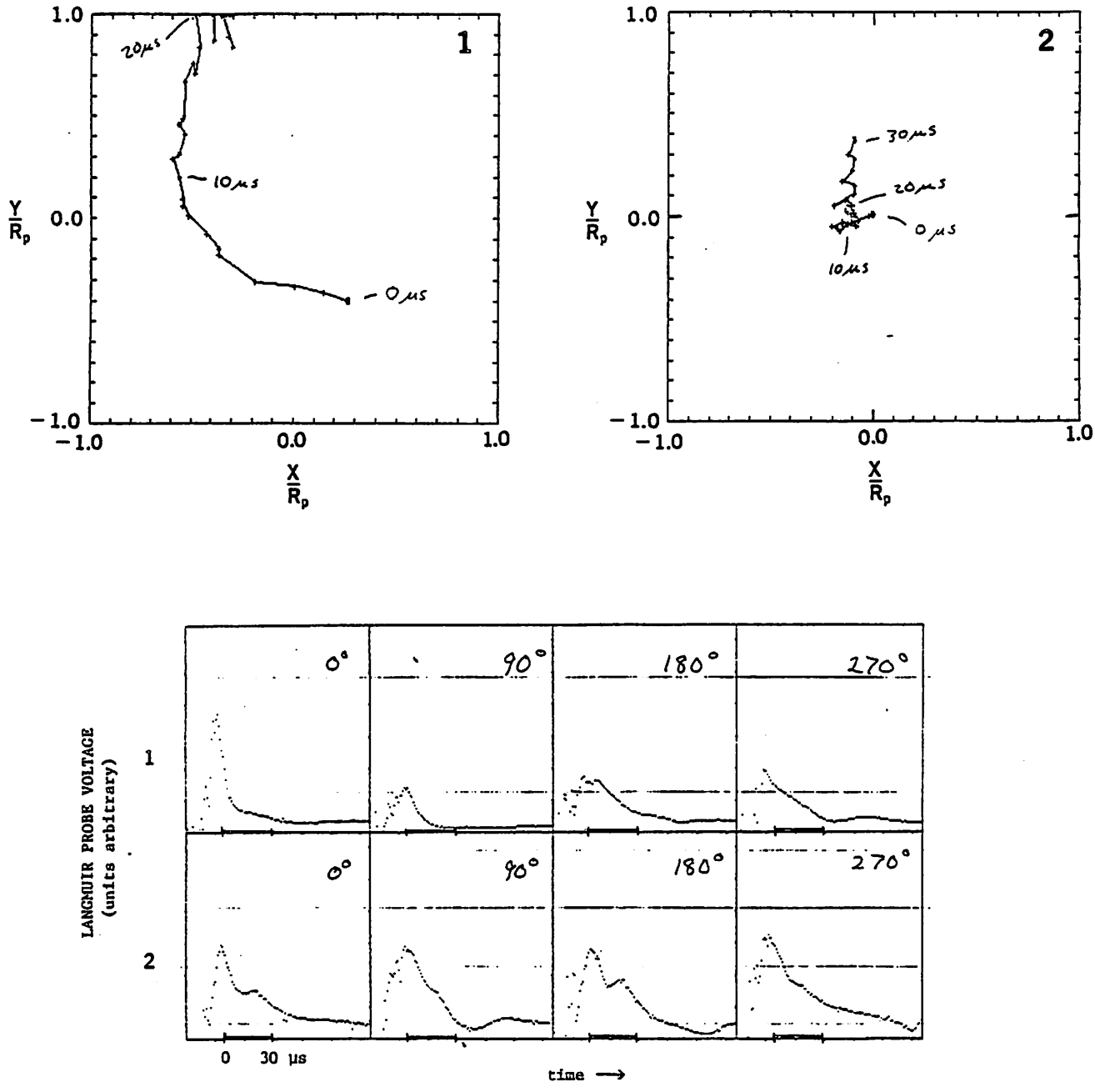

Figure 6: Centroid motion in a mirror cell (1) and near a stabilizing magnetic cusp (2) calculated from Langmuir probe data for a ballooning plasma instability.

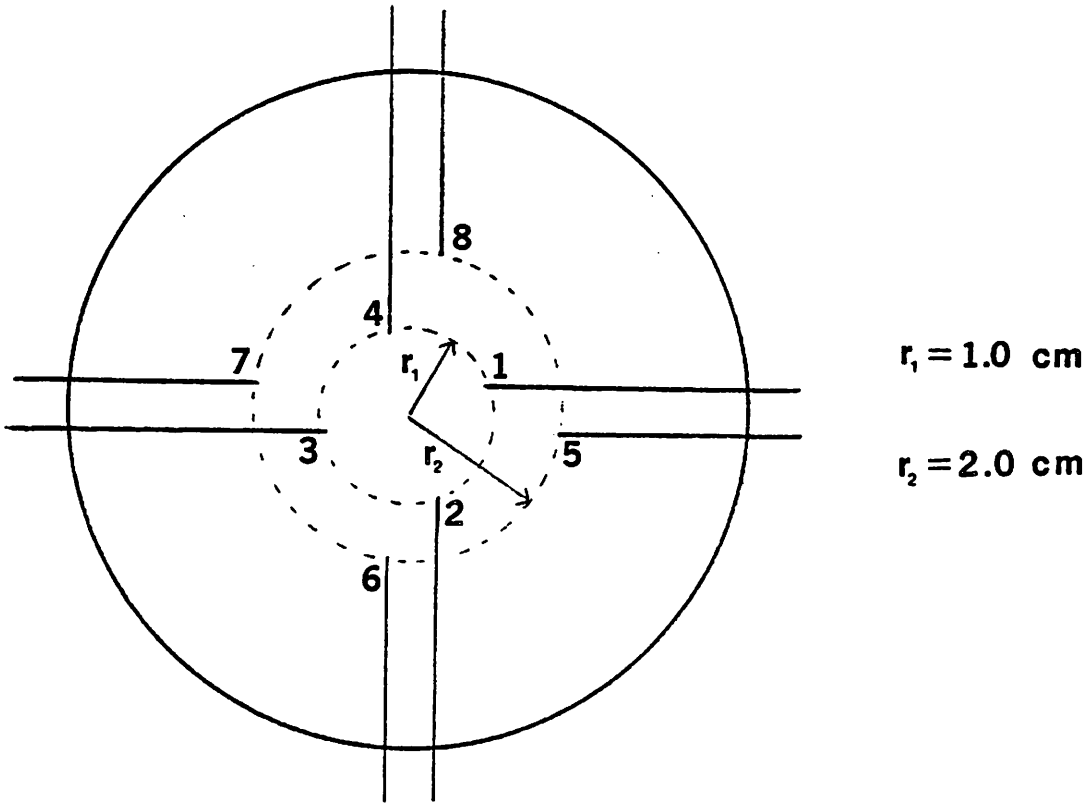

Figure 7: Floating probe array.

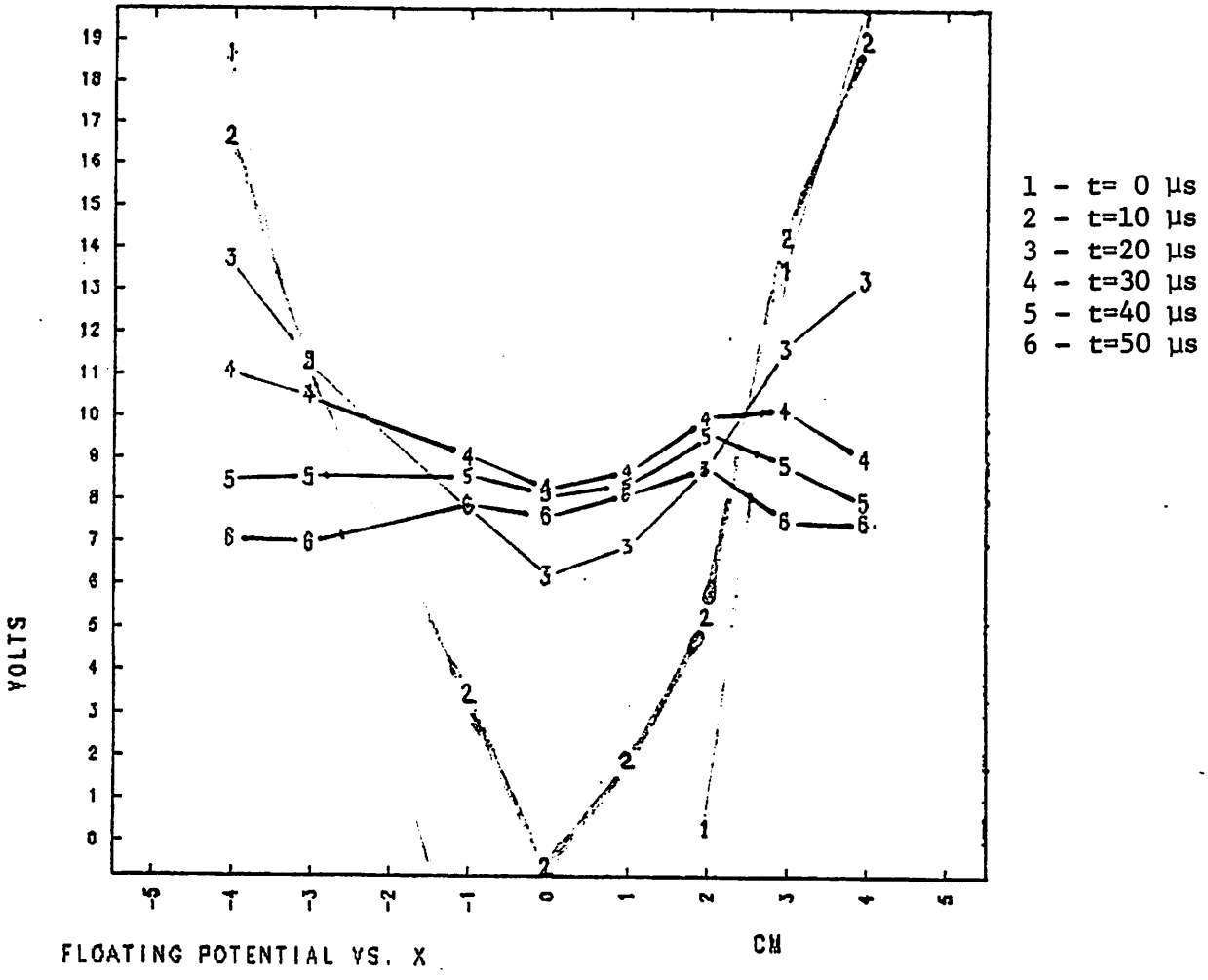

Figure 8: Floating potential profile for a stable shot.

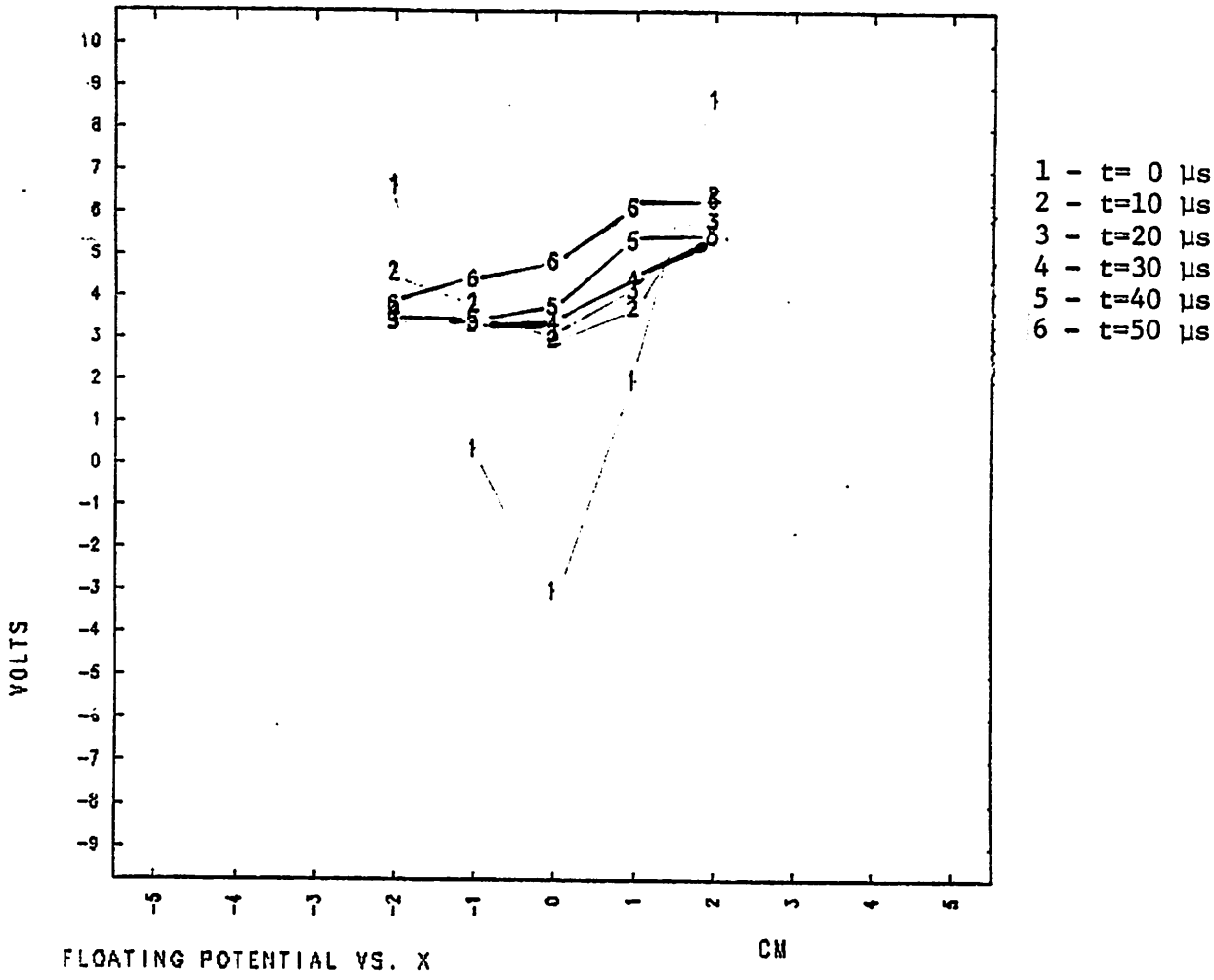

Figure 9: Floating potential profile for an unstable shot.

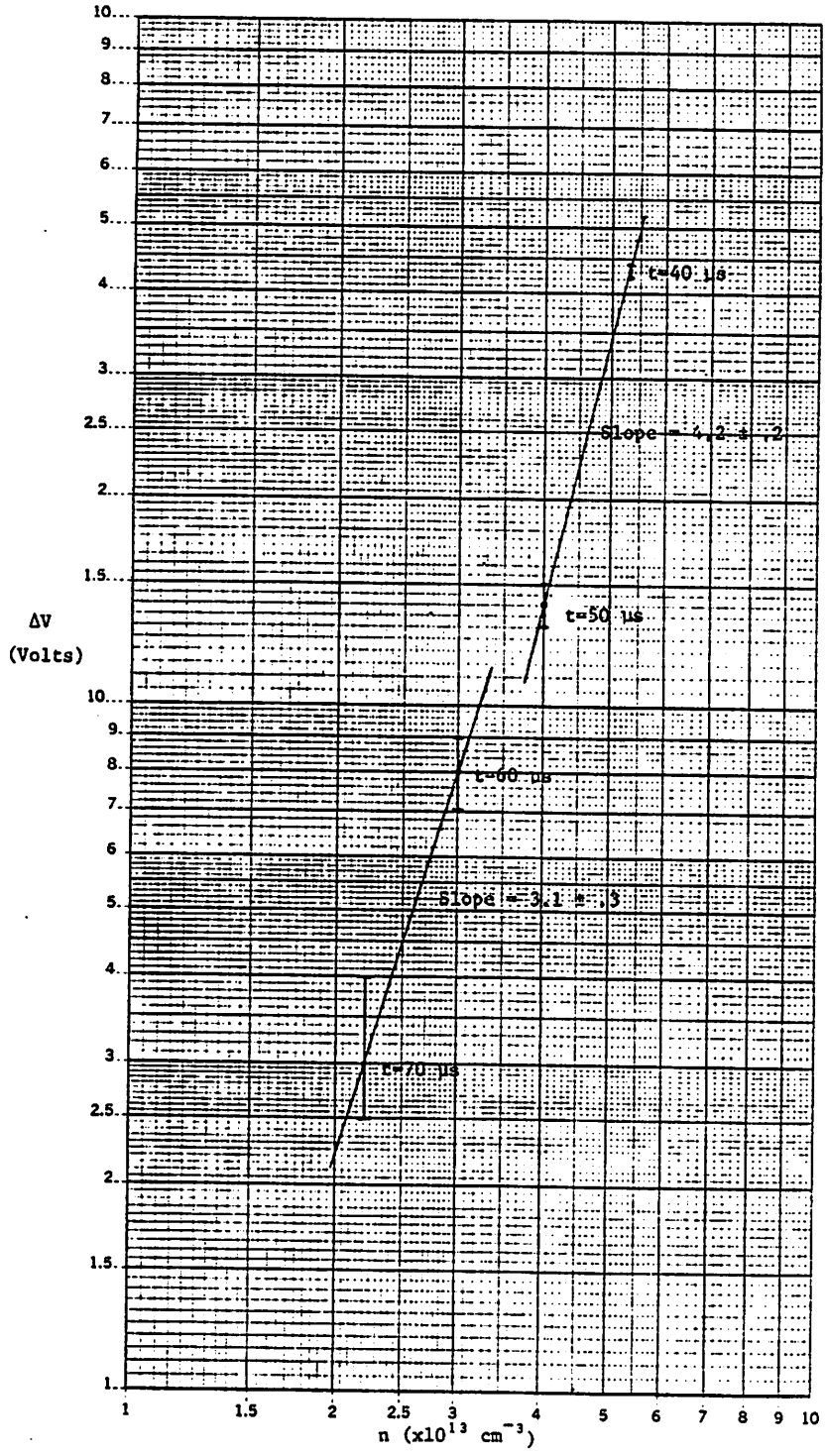

Figure 10: Scaling of radial floating potential variation with density (Floating potential difference measured between $x = 1.0$ and $x = 0.0$ cm).

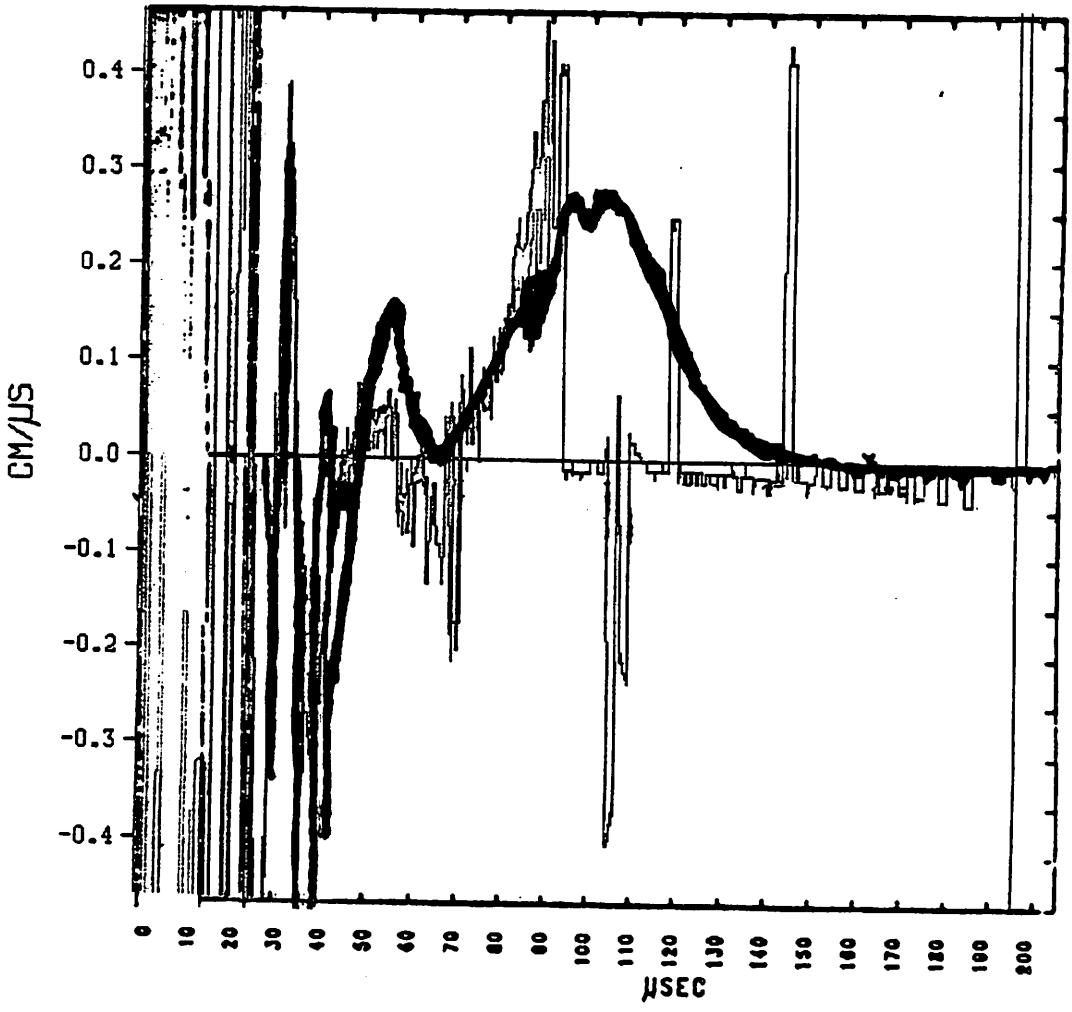

Figure 11: Velocity calculated from Langmuir probe array ion saturation current measurements (light trace) and floating probe array measurements (dark trace) for a flute-unstable configuration.

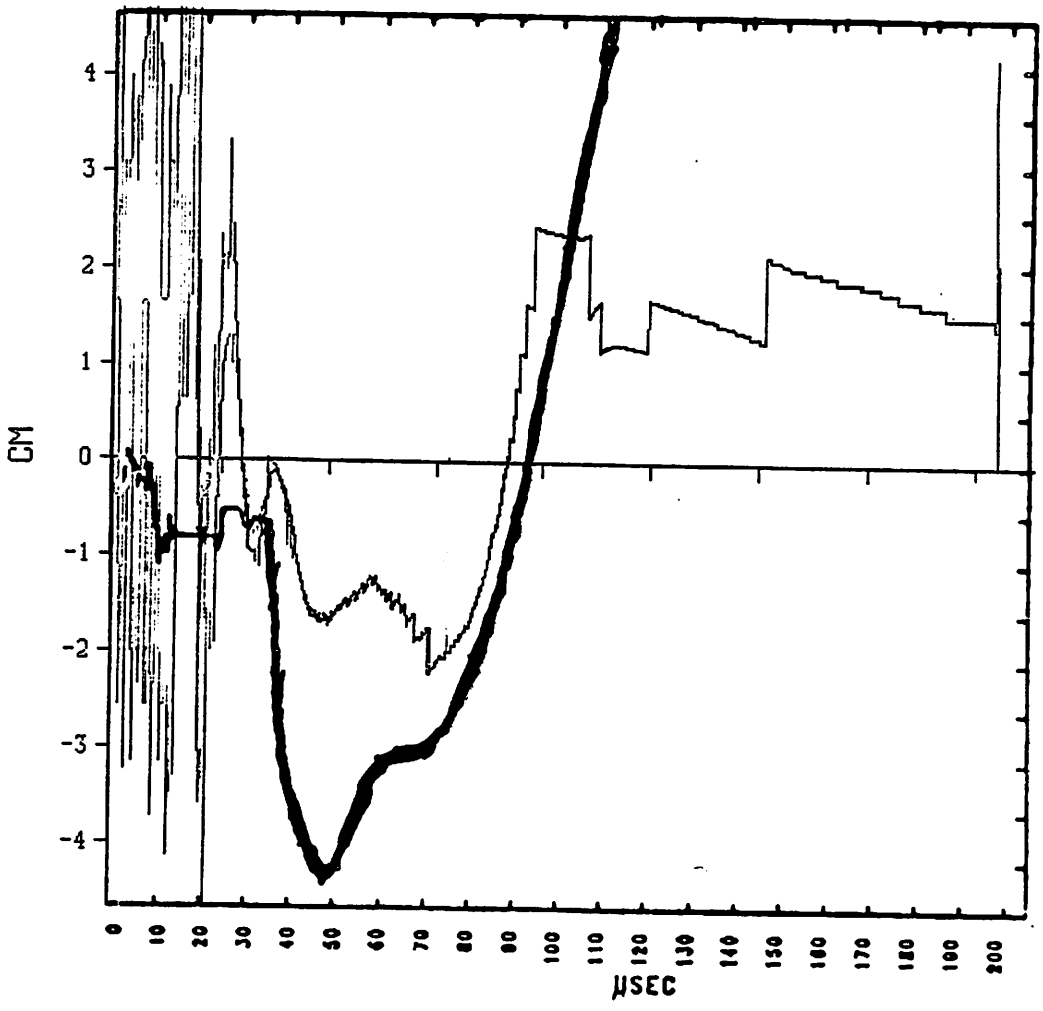

Figure 12: Integrated motion calculated from Langmuir probe array measurements (light trace) and floating probe array measurements (dark trace) using the same data as for the previous figure.

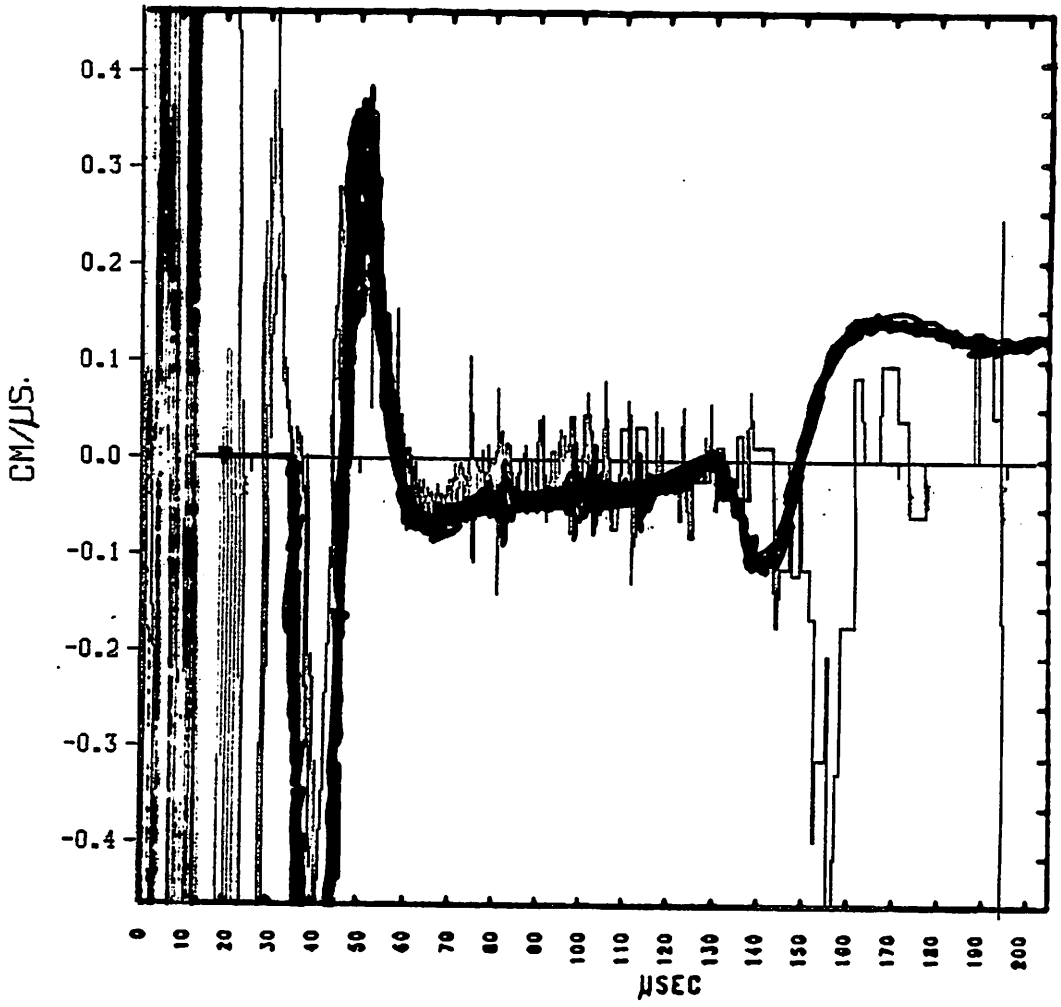

Figure 13: Velocity calculated from Langmuir probe data (light) and floating probe data (dark) for a magnetic configuration stabilized against flutes (ballooning behavior).

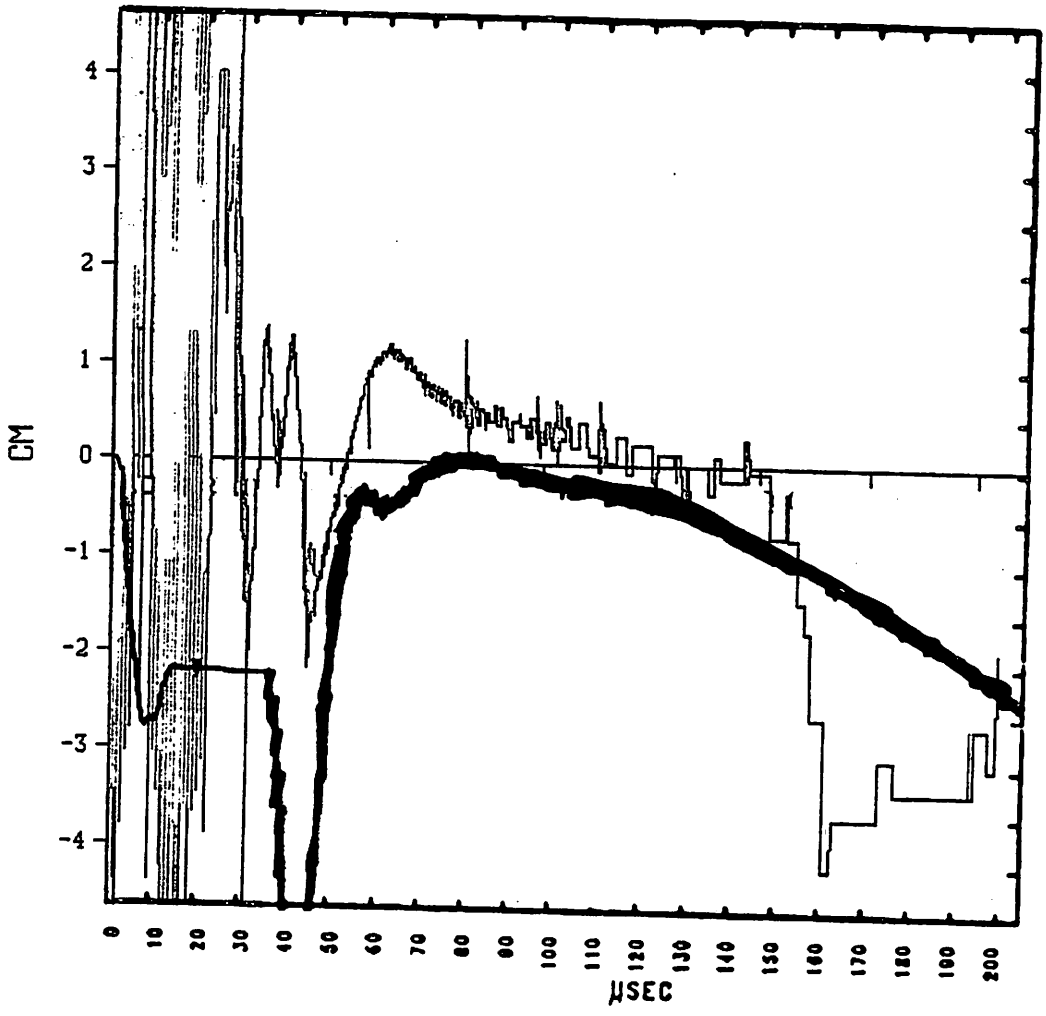

Figure 14: Integrated plasma motion calculated from Langmuir probe data (light) and floating probe data (dark) using the same data as for the previous figure.

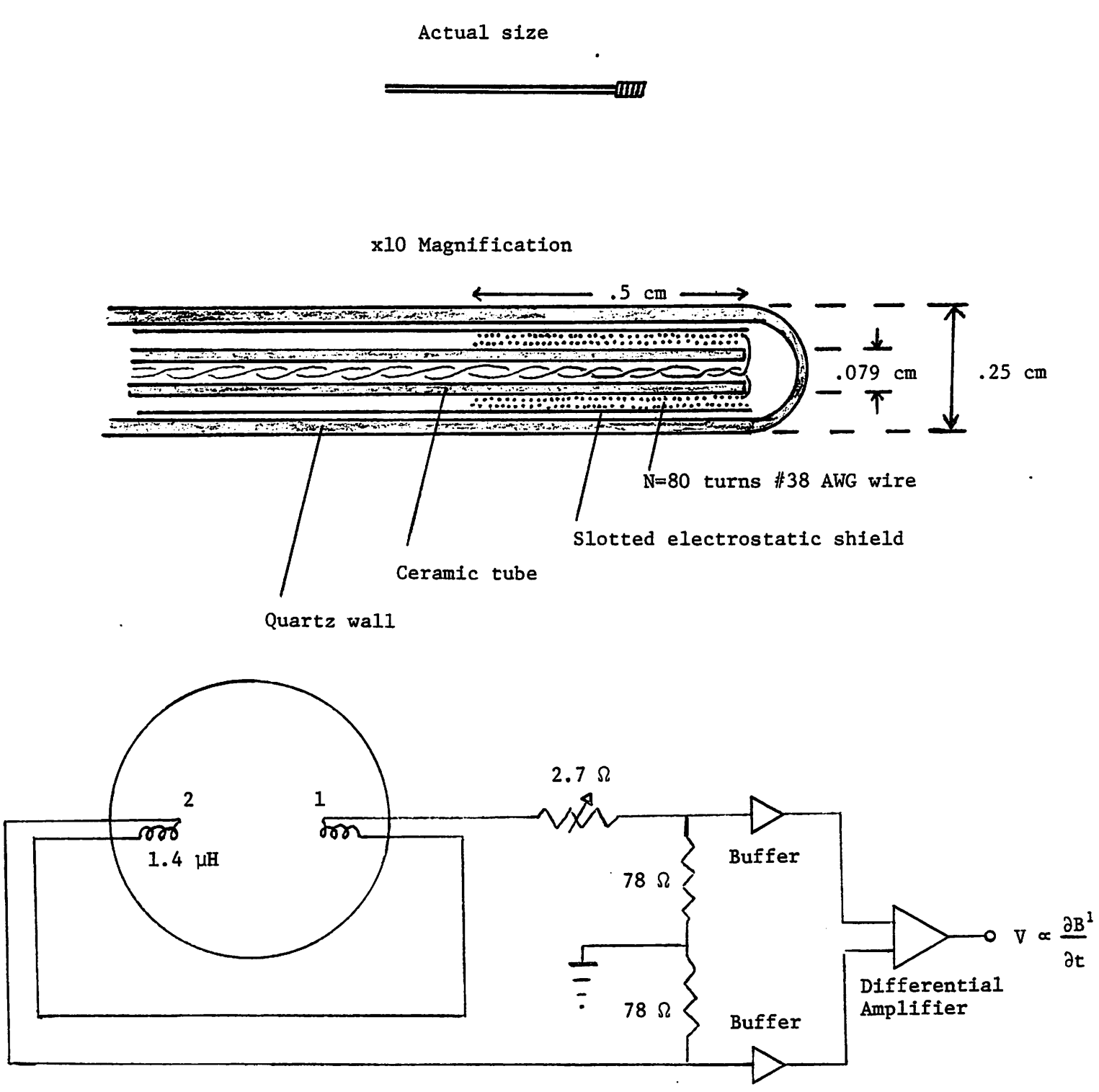

Figure 15: Magnetic probes.

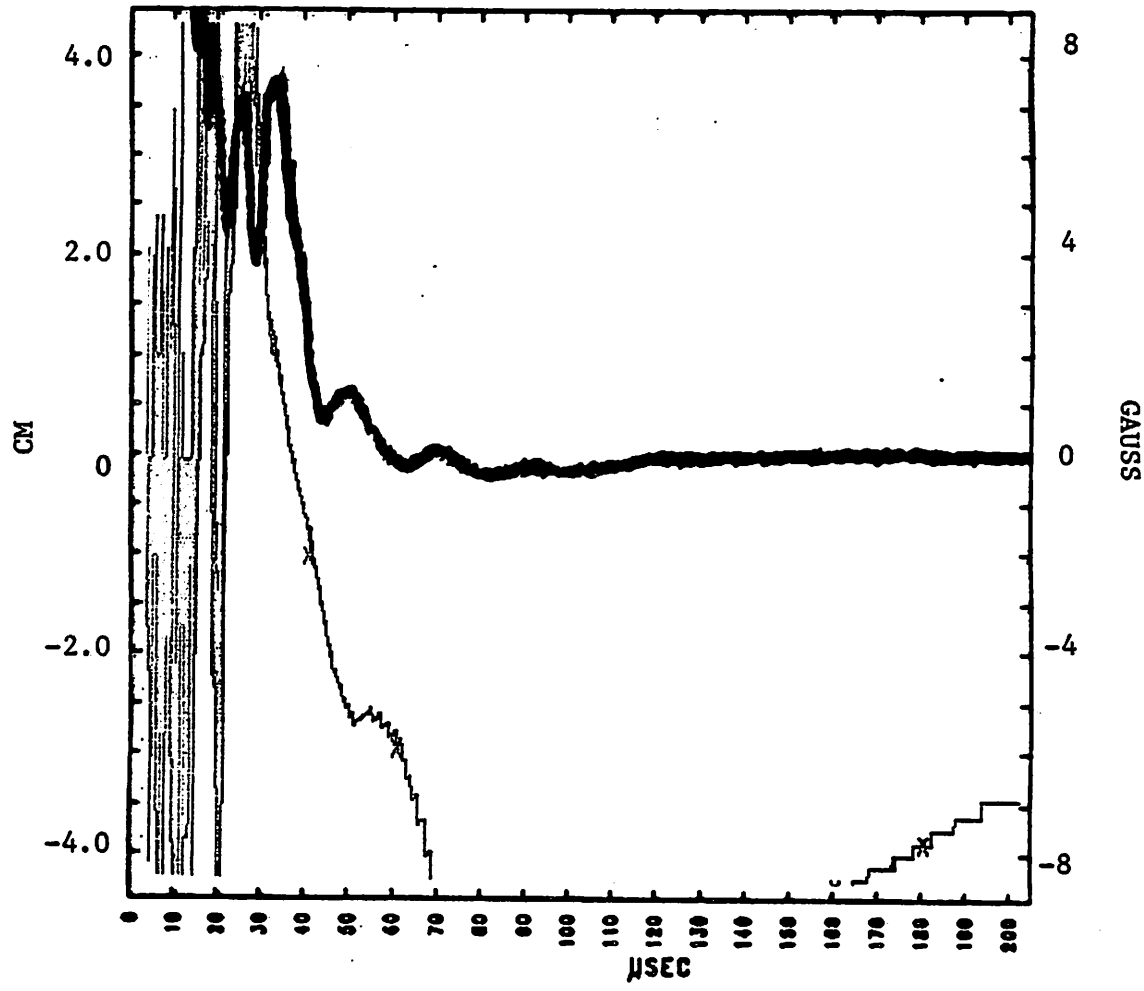

Figure 16: Perturbed magnetic field (dark) and plasma x-position (light) vs. time for flute mode.

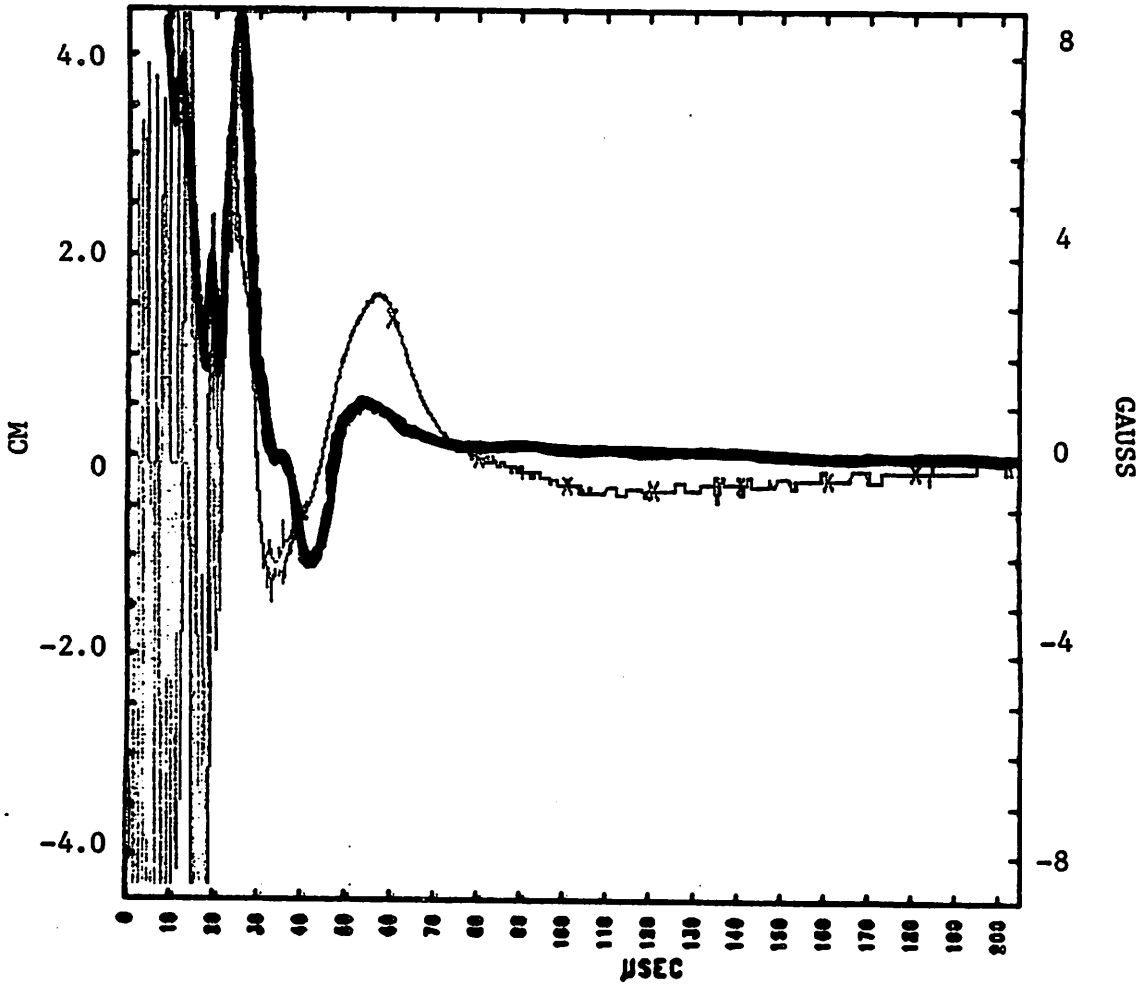

Figure 17: Perturbed magnetic field (dark) and plasma x-position (light) vs. time for ballooning mode.